

Journal of Materials Chemistry A

Materials for energy and sustainability

Accepted Manuscript

This article can be cited before page numbers have been issued, to do this please use: F. Meng, Q. Mo, J. Liu and N. Arai, *J. Mater. Chem. A*, 2026, DOI: 10.1039/D5TA10483A.



This is an Accepted Manuscript, which has been through the Royal Society of Chemistry peer review process and has been accepted for publication.

Accepted Manuscripts are published online shortly after acceptance, before technical editing, formatting and proof reading. Using this free service, authors can make their results available to the community, in citable form, before we publish the edited article. We will replace this Accepted Manuscript with the edited and formatted Advance Article as soon as it is available.

You can find more information about Accepted Manuscripts in the [Information for Authors](#).

Please note that technical editing may introduce minor changes to the text and/or graphics, which may alter content. The journal's standard [Terms & Conditions](#) and the [Ethical guidelines](#) still apply. In no event shall the Royal Society of Chemistry be held responsible for any errors or omissions in this Accepted Manuscript or any consequences arising from the use of any information it contains.

Adsorption kinetics of small molecules on FePt metallic electrode by classical molecular dynamics simulation

Fan Meng,^{*,†} Jialong Liu,[‡] Qiqi Mo,[‡] and Noriyoshi Arai[†]

[†]*Department of Mechanical Engineering, Keio University*

[‡]*Department of Physics and Electronics, School of Mathematics and Physics, Beijing University of Chemical Technology*

E-mail: mengfan@keio.jp

Abstract

Understanding how long reactants remain on catalytic surfaces (adsorption time) is essential for linking interfacial dynamics to overall reaction efficiency. In complex multistep systems such as the methanol oxidation reaction (MOR), the reaction pathways and surface poisoning are strongly related to the adsorption time and molecule orientation. By employing the molecular dynamics (MD) simulation method, the methanol, sulfuric acid and water molecules on the FePt alloy exposed to (001), (100) and (111) crystal planes were studied, thereby quantitatively defining and evaluating the adsorption time. Methanol exhibits the longest adsorption time, followed by sulfuric acid and water. Molecular conformation analysis further reveals two distinct interfacial regions: a 5 Å guiding layer, where methanol molecules initially approach the surface in a C-down configuration, and a 3 Å reaction layer, where the C-O bond reorient parallel to the surface. Facet-dependent analysis indicates that the (111) surface, with alternating Pt and Fe atoms, possesses the strongest adsorption capacity, where the adsorption



15 time for methanol is about 18 ps longer compared to the (001) facet. These findings
16 establish a unified framework that quantitatively connects atomic structure, adsorp-
17 tion time, and molecular orientation, which provides a time-resolved perspective for
18 the rational design of FePt-based electrocatalysts.

19 **Keywords** Methanol oxidation reaction; Adsorption time; FePt; Molecular dynamics sim-
20 ulation; Interfacial adsorption

21 Introduction

22 Among various sustainable energy technologies, direct methanol fuel cells have received ex-
23 tensive attention owing to their high energy efficiency, environmental impact, and efficient
24 portability.¹ Clarifying the mechanism of complex electrochemical reactions has always been
25 a challenge to improve the electrocatalytic performance.

26 Over the past two decades, first-principles calculations have played a pivotal role in elec-
27 trochemistry, providing fundamental insights towards the design principles of novel nano-
28 materials for energy devices such as fuel cells and lithium-ion batteries. A representative
29 example is the seminal work by Nørskov and co-workers, who in 2004 calculated the free-
30 energy landscape of the oxygen reduction reaction (ORR) on Pt surfaces and identified
31 the potential-determining step.² This thermodynamic approach, based on density functional
32 theory (DFT), excels at predicting thermodynamically stable adsorption configurations and
33 elucidating interfacial reaction mechanisms, thus guiding the experimental catalyst develop-
34 ment by enabling rapid screening of overpotentials. Zhou et al. computed the most stable
35 adsorption configurations of single volatile organic compound molecules on various metal ox-
36 ide surfaces,³ while Li et al. revealed that electron localization governs hydrogen adsorption
37 and hydride layer formation on Mg(0001) surfaces.⁴ However, the method inherently focuses
38 on reaction energetics at equilibrium and does not explicitly address kinetic effects such as
39 transition-state barriers. In reality, electrode processes are strongly influenced by interfacial



40 phenomena, including double-layer charging, local electric fields, and solvent-mediated pro-
41 ton transfer, all of which can alter kinetics substantially.⁵⁻⁷ Experimental techniques such
42 as in situ infrared spectroscopy and surface-enhanced Raman scattering have successfully
43 identified adsorbed species on catalyst surfaces. But, these methods inherently average over
44 surface aggregation and time scales, obscuring the transient adsorption/desorption dynamics
45 at individual active sites.

46 Another method, classical molecular dynamics (MD), is emerging as an important sup-
47plementary way to simulate the dynamic process in the actual reaction. MD simulations can
48 calculate interfacial processes involving multiple molecules and thousands of atoms, provid-
49ing a realistic statistical representation of the catalytic environment. Moreover, MD resolves
50 atomic trajectories on the picosecond timescale, enabling direct observation of adsorption,
51 diffusion, and desorption events. These features make MD a powerful tool for investigat-
52ing kinetic phenomena that govern surface reactions. True electrochemical interfaces are
53 characterized by the presence of an interfacial electric field and a solution phase. Further,
54 differences in electrode surface charge directly lead to changes in the electrochemical bilayer
55 structure, which brings about changes in reaction kinetics as well as a variety of other pos-
56sibilities. The presence of the solution phase, on the other hand, promotes proton transfer
57 and lowers the reaction energy barrier. The femtosecond precision makes MD simulations
58 powerful to investigate the kinetic behavior. For example, mean square displacement (MSD)
59 analysis, diffusion coefficient (D), and radial distribution functions (RDFs, $g(r)$) have been
60 widely used to characterize molecular mobility and structural ordering near surfaces.⁸⁻¹¹ The
61 time scales of adsorption behavior of reactants, particularly their adsorption time (τ_{ads}) at
62 active sites, emerge as a critical yet underexplored kinetic determinant. This time dimen-
63sion dictates whether intermediate species can undergo complete transformation or desorb
64 prematurely, ultimately controlling reaction selectivity and efficiency.^{12,13}

65 Prior studies indicate that methanol, sulfate/sulfuric acid species, and water play distinct
66 interfacial roles and exhibit different adsorption strengths on Pt-based electrodes; however,



67 their time-resolved adsorption behavior has not been quantitatively established. Surface
68 structure can significantly influence the adsorption/desorption thermal dynamics, leading
69 to various adsorption behaviours of different molecular species.^{14,15} However, a direct, time-
70 resolved description of adsorption events is not acquired at the molecular level. This gap
71 motivates our analysis of adsorption time distributions across species and facets, which are
72 quite important to explore the complex multistep reactions such as MOR.

73 In this work, all-atom classical molecular dynamics simulations are employed to elucidate
74 the relationship between electrode surface structure and the adsorption behavior of methanol
75 on FePt electrocatalysts with different facets. The adsorption time, a quantitative descriptor,
76 is quantitatively determined, which can provide an intuitive, time-resolved perspective on
77 small-molecule adsorption at catalytic interfaces. Furthermore, the posture configurations of
78 molecules near the surface are analyzed. The study of dynamic processes with MD simulation
79 offers new insights into the molecular-level dynamics of MOR and helps design Pt-based
80 nanomaterials with specific microstructures.

81 Method

82 Simulation model

83 Simulations were performed with the GROMACS package.¹⁶ The experimental electrolyte
84 used in the reference study consisted of 0.5 M H₂SO₄ and 1 M CH₃OH.¹⁷ Based on the
85 experimental data, the methanol- to-sulfuric acid ratio was set to 2:1. To maintain a man-
86 ageable computational cost, the number of water molecules was moderately reduced. The
87 liquid phase box is comprised of 2,000 methanol molecules, 1,000 sulfuric acid molecules, and
88 30,000 water molecules. After appropriately reducing the number of water molecules, the
89 final concentration of methanol was approximately 1.8 - 2 mol/L, and the ratio of methanol
90 to sulfuric acid was 1:2. The lateral dimensions of the simulation box (x and y) were fixed at
91 approximately 13 nm to match the electrode slab size. The box length along the z-direction



92 was then determined from the experimental density and the total number of molecules in
93 the system. Water was represented by the TIP4P model, and all intermolecular interactions
94 were described using the General AMBER Force Field version 2 (GAFF2).¹⁸ The force-
95 field combination adopted here has been evaluated in previous studies against solvation and
96 cross-solvation free energies in aqueous and organic environments, providing prior support
97 for its applicability in the present simulations.^{19,20} The FePt electrode atoms were mod-
98 eled using Lennard-Jones parameters derived from the Universal Force Field (UFF).²¹ The
99 Lennard-Jones parameters used in the simulations correspond to the values implemented in
100 the GROMACS topology. Cross interactions between different atom types were calculated
101 using the Lorentz-Berthelot combining rules:

$$\sigma_{ij} = \frac{\sigma_i + \sigma_j}{2} \quad (1)$$

$$\varepsilon_{ij} = \sqrt{\varepsilon_i \varepsilon_j} \quad (2)$$

103 where σ_{ij} and ε_{ij} are the Lennard-Jones size and energy parameters between atom types i
104 and j , respectively.

105 After energy minimization and equilibration, production runs were conducted in the
106 NVT ensemble at 298 K with a time step of 1 fs. Temperature was controlled using the
107 V-rescale thermostat, and atomic charges were assigned with the Gasteiger method.²² Long-
108 range electrostatic interactions were treated using the particle mesh Ewald (PME) method,
109 while short-range electrostatic and van der Waals interactions were truncated at 1.13 nm.
110 All bonds involving hydrogen atoms were constrained using the LINCS algorithm. For each
111 system, five consecutive NVT simulations were performed, each lasting 10 ns, giving a total
112 simulation time of at least 50 ns. The trajectory from the final 10 ns run was used for analysis.
113 The trajectory from the final 10 ns was used for analysis. The molecular trajectories were
114 analyzed and visualized with the OVITO software²³ (Fig.1).

115 The lattice parameters of the FePt surface alloy were obtained from the Materials Project



116 database (MP-1198813),^{24,25} as listed in Table 1. The surface orientations were constructed
117 based on the L1₀-phase structure (JCPDS 43-1358).²⁶ Three slab models exposing the (100),
118 (001), and (111) surfaces were constructed for the simulations. The atomic coordinates of
119 the FePt electrode slabs were generated using in-house code based on the crystallographic
120 lattice parameters and surface orientations described above. For the (001) and (100) facets
121 of FePt, the topmost atomic layer can be terminated by either pure Pt atoms or pure Fe
122 atoms because of the layered L1₀ ordering. Consequently, two distinct surface terminations,
123 Pt-terminated and Fe-terminated surfaces, naturally arise for these orientations. In contrast,
124 the (111) surface exposes a mixed Fe-Pt atomic layer, making a single, compositionally mixed
125 termination. Under periodic boundary conditions, the simulation cell forms a surface-liquid-
126 surface arrangement. For the FePt (001) and (100) slabs, this arrangement naturally gives
127 rise to one Pt-terminated interface and one Fe-terminated interface, which are analyzed
128 separately in the following sections. The atoms of the electrode slab were kept fixed during
129 the simulations. Detailed force-field parameters and atomic charges used in the simulations
130 are provided in the Supporting Information section 1.

131 Result & Discussion

132 Density distribution analysis

133 The distribution of molecules near the surface strongly affects the kinetic dynamics in electro-
134 catalysis, which further influences the formation of a double electrical layer. Also, previous
135 studies have found that the electrode area, surface morphology, and atomic arrangement in-
136 fluence the molecules attachment and movement.^{27,28} As shown in Fig. 2, for the Pt-terminal
137 surface on the left, a pronounced methanol peak appears within the first 3.8Å, confirming
138 strong methanol adsorption. A minor sulfuric acid peak is also present for the Pt-terminal
139 surface. At the Fe interface, the absence of a density peak for sulfuric acid indicates that
140 it does not adsorb and is weakly repelled by Fe sites. Water and methanol overlap within



141 4.1 Å of the Pt surface. Previous studies have also reported that competitive adsorption on
142 the catalyst surface.¹²

143 Comparisons across the three different Miller index surfaces reveal no significant differ-
144 ences in the methanol and water density profiles, while the sulfuric acid density is notably
145 lower near the (111) facet. At a distance of 3 Å from the surface, the sulfuric acid den-
146 sity decreases from approximately 145 kg m⁻³ on the (001) surface to 71 kg m⁻³ on the
147 (111) surface, consistent with stronger sublayer Fe involvement and the associated repulsive
148 interaction at this interface.

149 Fig. 2 (d-f) shows the density distributions of each species on the Pt-contact surface
150 with different Miller indices. As shown in Fig. 2(d) and (f), the methanol and water density
151 profiles for the three facets indicate that variations in surface orientation have little influence
152 on surface adsorption behavior. Fig. 2(e) reveals that the three terminal layers affect the
153 sulfuric acid density distribution, as sulfuric acid is repulsion from Fe sites. The sulfuric acid
154 density decreases with increasing Fe exposure at the surface, indicating that sulfuric acid
155 molecules are repelled by Fe sites. A minor peak appears on the (001) surface, where the
156 subsurface Fe layer lies farther from the surface. In this configuration, the weaker repulsive
157 influence of Fe atoms allows limited sulfuric acid accumulation, resulting in the small peak
158 observed. The sulfuric acid density on the (100) facet, which exhibits a higher degree of
159 Fe exposure in the subsurface layer, is lower than that on the (001) facet. On the (111)
160 surface, where surface Fe atoms are fully exposed, the sulfuric acid peak vanishes entirely.
161 On the (111) surface, the adsorption of sulfuric acid becomes less favorable, thereby allowing
162 preferential accumulation of methanol and water molecules at the surface.

163 The density profiles provide valuable information about molecular aggregation near the
164 surface. These analyses offer quantitative insights into interfacial composition, solvation
165 structure, and the thickness of the equilibrium molecular layers, which are highly valuable
166 for guiding experimental studies on surface adsorption and catalyst-electrolyte interactions.
167 However, these static profiles do not directly reflect the time-scale aspect of adsorption.



168 The duration of molecular residence at active sites is particularly important for multistep
169 reactions such as MOR, where longer adsorption times facilitate more complete reaction
170 pathways. Therefore, the adsorption times of each species were analyzed to obtain a more
171 intuitive, time-resolved understanding of the adsorption behavior.

172 Adsorption Time

173 The adsorption time of reactants kinetically governs the MOR, and surface poisoning results
174 from an imbalance of reactant adsorption on the catalyst surface.^{29–31} Such an imbalance
175 typically results in excessively long adsorption times of CO-producing intermediates or in-
176 sufficient adsorption of OH-supplying species, leading to incomplete oxidation pathways. In
177 other words, surface poisoning can be mitigated either by shortening the adsorption time
178 of poisoning precursors or by extending the adsorption time of species required to remove
179 them. Therefore, adsorption time serves as a key descriptor for understanding MOR kinetics,
180 as prolonged adsorption at the solid-liquid interface facilitates the complete conversion of
181 intermediates such as CO. Through classical molecular dynamics simulations, we established
182 a method to directly quantify adsorption time. To determine an appropriate adsorption dis-
183 tance, ten methanol molecules were randomly selected from the entire simulation box, and
184 their center-of-mass positions were tracked along the z-axis. These trajectories show that
185 adsorption events consistently occur within 1 nm of the catalyst surface, consistent with
186 the density distribution analysis. Therefore, a 1 nm range was adopted as the effective ad-
187 sorption region. This choice is also physically justified, as van der Waals interactions in the
188 GAFF2 force field are explicitly evaluated only within the Lennard-Jones cutoff of 1.13 nm.
189 Molecules inside 1 nm are thus subject to the dynamical influence of the surface, whereas
190 those farther away experience negligible direct interactions.

191 To exclude transient collisions-instances where molecules briefly enter the adsorption
192 region and immediately escape, we defined a molecule as “adsorbed” only if it remained
193 within 1 nm of the surface for longer than 5 ps. This criterion ensures that only meaning-



194 ful adsorption events are included in the analysis. This criterion is determined through a
195 convergence analysis. Smaller distance thresholds (e.g., 3 Å) result in too few adsorption
196 events with residence times exceeding the cutoff, leading to unstable statistics. The distance
197 and time criteria are therefore gradually increased until the adsorption-time distributions
198 converge, yielding 1 nm and 5 ps as robust thresholds for defining meaningful adsorption
199 events. It should be noted that the 1 nm criterion used in the adsorption-time analysis does
200 not represent direct surface contact in the strict Helmholtz-layer sense, but rather defines a
201 near-surface residence region for kinetic analysis.

202 The adsorption time distributions of methanol, sulfuric acid, and water molecules are
203 shown in Fig. 3(a-c). The adsorption time distributions of methanol, sulfuric acid, and
204 water were fitted using single Gaussian functions of the form

$$g_i(x) = A_i \exp\left[-\frac{(x - \mu_i)^2}{2\sigma_i^2}\right], \quad i = 1, 2, 3 \quad (3)$$

205 to quantify their average adsorption times and temporal dispersions. The fitted parameters
206 are listed in the Table. 2. Considering the Pt-terminal surface, firstly, methanol, as the
207 main reactant, exhibits the longest adsorption times, ensuring sufficient surface contact for
208 reaction progression. Sulfuric acid molecules display middle-range adsorption times. Rather
209 than acting as a direct reactant in MOR, they primarily serve to maintain an acidic, ion-
210 conductive environment that facilitates charge transport in the electrolyte. In addition,
211 adsorbed sulfate species partially occupy surface sites and modulate the local electronic
212 environment of the catalyst surface, thereby helping to suppress undesired side processes
213 such as excessive CO adsorption and surface oxidation of the metal. Water molecules, in
214 contrast, show the shortest adsorption times, as they must rapidly participate in surface
215 reactions and continuously replenish OH⁻ ions. This distribution reflects the functional
216 roles of the three species during MOR and supports the reliability of our simulation model.
217 Notably, this work quantitatively characterizes—for the first time—the adsorption durations



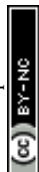
218 of individual reactants in the FePt-catalyzed MOR system, providing an intuitive comparison
219 of how different reactants interact with the surface on distinct time scales.

220 Facet-dependent adsorption behavior further reveals the structure-function relationship
221 of FePt surfaces. A comparison of the (001) and (100) facets indicates that the average
222 methanol adsorption time on the (100) surface is 7.8 ps longer (Table 2). Previous studies
223 have demonstrated that facet engineering and doping engineering can substantially influence
224 the adsorption behavior of reactants and intermediates, because different crystal planes ex-
225 pose distinct atomic coordination environments, while dopants modify the local geometric
226 structure at the catalyst surface.¹⁴ In our FePt system, the Pt-Pt spacing on the (001) facet
227 is 2.73 Å, while the Pt-Pt spacing on the (111) facet is 3.74 Å. This variation in surface lattice
228 strain enables subsurface Fe atoms to participate more effectively in interfacial interactions
229 with methanol, thereby extending the adsorption time.

230 In addition to compositional effects, lattice strain in Pt-based catalysts has been reported
231 to modulate the methanol oxidation pathway by tuning the stability of reaction intermedi-
232 ates.³² Zeng et al. shows that lattice contraction stabilizes formate-related intermediates,
233 while moderate strain enhances CO₂ production through CO intermediates and mitigates
234 CO poisoning.³³ Pt provides stable MOR sites but is susceptible to CO poisoning, and Fe
235 enhances water adsorption and assists in the removal of CO intermediates.^{29,34}

236 Among all facets, the (111) surface shows the most optimal adsorption characteristics.
237 Its alternating Pt-Fe atomic surface arrangement allows Fe to contribute more significantly
238 to adsorption, while Pt serves as the primary catalytic site for MOR. This configuration
239 integrates the complementary roles of Pt and Fe, with Fe modulating methanol and water
240 adsorption. Notably, methanol adsorption on the (111) surface is 17.9 ps longer than on the
241 (001) surface, highlighting the rationality of FePt as a methanol fuel cell electrode material.
242 The (111) facet maximally leverages the synergistic functions of Fe and Pt, thereby enhancing
243 catalytic performance.

244 Given the crucial role of CO as a poisoning intermediate in MOR, we further performed



245 adsorption-time analysis for CO on the FePt(111) surface. As shown in Fig. 3(d), CO exhibits
246 a much longer adsorption duration of 70.4 ps, substantially longer than that of methanol.
247 Such prolonged residence enables CO to occupy active Pt-Fe interfacial sites persistently,
248 thereby blocking methanol adsorption and hindering the overall reaction progress. This
249 finding is consistent with in situ spectroscopic observations showing that CO_{ads} can persist
250 on Pt-based surfaces even when conventional electrochemical indicators suggest minimal
251 poisoning, highlighting the importance of resolving adsorption behavior beyond current-
252 based metrics.³⁵

253 In contrast to the methanol-only simulations, where extending methanol residence did
254 not noticeably shorten the adsorption times of sulfuric acid and water, the CO-loaded system
255 shows a distinctly different behavior. In the presence of CO, both sulfuric acid and water
256 display significantly reduced adsorption durations, indicating strong competitive adsorption
257 between CO and these two species. Because sulfuric acid modulates the interfacial ionic en-
258 vironment and water provides hydroxyl radical pathways, the suppression of their adsorption
259 further aggravates MOR deactivation. These results demonstrate that excessively strong CO
260 adsorption not only blocks methanol but also disrupts the adsorption balance of coexisting
261 electrolytes, thereby amplifying CO poisoning effects.

262 To further understand the interfacial behavior of poisoning intermediates, we additionally
263 analyzed the density distribution of CO along the surface-normal direction (Fig. S1). CO
264 exhibits a pronounced density enhancement near the FePt surface, with a steep increase in the
265 interfacial region of approximately 0.6–0.9 nm from the surface. Compared with methanol
266 under similar conditions, the CO density profile shows a broader interfacial peak, indicating
267 that CO is more strongly localized near the electrode and forms a thicker adsorption layer.
268 In contrast to the methanol-containing system, where methanol and water densities increase
269 more synchronously within about 0.6–1.0 nm, in the CO-containing system H₂SO₄ and H₂O
270 remain relatively low in the 0.6–0.8 nm region and increase more noticeably only at larger
271 distances. These results are consistent with the relatively long adsorption times of CO and



272 support its role in surface poisoning during the MOR process. The growth rate of the CO
273 density profile is substantially higher than that of H₂O, whereas the slope for CH₃OH is
274 comparable to that of H₂O. This suggests that, under the present molecular composition,
275 CH₃OH and H₂O show similar interfacial access and residence behavior, which may be
276 favorable for methanol oxidation at the surface. In contrast, the much steeper increase for
277 CO indicates a stronger tendency for interfacial accumulation, consistent with its slower
278 removal or oxidation at the interface. More detailed density-profile analysis is provided in
279 the Supporting Information section S3.

280 Generally speaking, the adsorption time distribution obtained in this work is consistent
281 with the mechanistic requirements of MOR: methanol exhibits the longest adsorption time
282 to ensure sufficient surface residence for oxidation, sulfuric acid maintains the interfacial
283 ionic environment with intermediate-duration adsorption, and water molecules display the
284 shortest adsorption times due to their rapid transport across the interface. Furthermore, our
285 additional analysis of CO reveals that its excessively long adsorption time severely perturbs
286 this balance, displacing both sulfuric acid and water from the surface and thereby amplifying
287 poisoning effects. These findings demonstrate that facet selection and Fe incorporation
288 effectively tune molecular adsorption and interfacial dynamics, providing quantitative guid-
289 ance for the rational design of FePt-based bifunctional electrocatalysts. Although previous
290 studies have qualitatively suggested differences in adsorption behavior among reactants, the
291 present work provides a quantitative, time-resolved description of these adsorption processes,
292 helping to clarify how individual species interact and compete at the catalytic interface.

293 **Molecular conformation and its Role in MOR**

294 Prior experimental and spectroelectrochemical studies have shown that methanol oxidation
295 on Pt-based surfaces proceeds through multiple surface intermediates, including CO-related
296 pathways, and that the interfacial molecular environment can significantly influence elec-
297 trocatalytic behavior.^{36–38} While adsorption time analysis establishes how long reactants



298 remain in contact with the surface and validates the time dimension of the MOR pathway, it
299 does not reveal how molecules actually interact with the surface during this adsorption time.
300 To address this complementary aspect, an examination of the contact modes of methanol
301 molecules near the electrode surface is carried out. Two primary configurations were iden-
302 tified: C-down and O-down. In the C-down configuration, the carbon side of methanol
303 approaches the surface first, which may be more conducive to interactions associated with
304 C-H activation. In contrast, the O-down configuration brings the hydroxyl group closer
305 to the surface and may therefore be more favorable for interactions associated with O-H
306 activation.³⁹ This spatial-orientational perspective, when combined with adsorption lifetime
307 analysis, provides a more complete molecular-level understanding of the reaction mechanism.

308 To quantitatively describe these orientations, we defined $\cos\theta$ as the angle between the
309 C-O bond vector of methanol and the positive z-axis perpendicular to the surface. The
310 orientation analysis was carried out for two surface layers with thicknesses of 5 Å and 3 Å
311 (Fig. 4(a,b)). These distances were selected with reference to the classical Helmholtz double-
312 layer model that describes the interfacial structure of electrochemical systems. In classical
313 electrochemical interface theory, the electrode-electrolyte boundary is described by an elec-
314 trical double layer (EDL) composed of the inner Helmholtz plane (IHP) and outer Helmholtz
315 plane (OHP) among others.⁴⁰ The IHL is understood to consist of molecules and specifically
316 adsorbed ions in direct contact with the electrode surface, extending on the order of a few Å
317 from the interface.⁴¹ Accordingly, we selected 3 Å as the boundary for the reaction-layer
318 and 5 Å for the guiding-layer analysis in our molecular-dynamics model. The choice of 3 Å
319 approximately corresponds to the molecular dimension of methanol,⁴² such that this layer
320 represents the first adsorbed molecular layer in direct contact with the catalyst surface. The
321 5 Å region was selected to capture the second-layer configurations, which are important for
322 understanding how molecular orientations in the outer layer transform into the first contact
323 layer. Because interfacial molecules are not arranged in perfectly discrete layers but rather in
324 a partially overlapping arrangement, thus 5 Å provides a more realistic boundary than 6 Å.



325 At 5 Å, most methanol molecules exhibit a C-down orientation. However, closer to the sur-
326 face, in the 3 Å first contact layer, the $\cos \theta$ distribution becomes nearly Gaussian, indicating
327 that methanol molecules preferentially lie flat on the surface. Such lying-flat configurations
328 maximize the contact area with the surface, representing a pre-reaction state in which both
329 C-down and O-down pathways are accessible. The prevalence of C-down orientations in the
330 5 Å layer also provides a kinetic explanation for the well-known difficulty in removing CO
331 intermediates during the MOR process.

332 We define the 5 Å region as a guiding layer, where C atoms act as anchor points due
333 to their stronger interaction with the surface, driving the methanol molecules toward the
334 surface. Upon entering the 3 Å first contact layer, the molecules reorient to a flat config-
335 uration, preparing for bond break and subsequent MOR steps. This two-layer adsorption
336 mechanism illustrates how initial C-down attraction facilitates molecular migration, while
337 surface-parallel orientations at the first contact layer enable efficient reaction pathways with
338 minimized CO formation. At this point, the adsorption mechanism diagram of the pre-
339 MOR reaction from a classical molecular dynamics perspective is shown in Fig. 5. The
340 interfacial region above the FePt surface is divided into a reaction layer and a guiding layer.
341 In the guiding layer, reactant molecules are kinetically steered toward the surface, where
342 molecular approach and initial orientation are governed by long-range surface interactions.
343 Upon entering the reaction layer, molecules are in direct contact with surface atoms, adopt
344 surface-parallel configurations, and undergo orientation reorganization that facilitates bond
345 activation and subsequent reaction steps. This two-layer framework provides a unified in-
346 terpretation of the adsorption-time statistics and orientation distributions observed in the
347 classical molecular dynamics simulations.

348 We also analyzed the contact configurations of CO at both 5 Å and 3 Å from the surface
349 (Fig. 4(c,d)). In contrast to methanol, CO exhibits a dominant O-down orientation in
350 both regions. Because the O atom is more electronegative, O-down contact suppresses
351 electron transfer into the antibonding orbitals of CO, thereby limiting C-O bond activation



352 and hindering its further oxidation. As will be shown in our DFT analysis, CO's C-down
353 configurations are thermodynamically more stable than O-down ones (Fig. 6(f, l)). In the
354 C-down geometry, the carbon atom can interact more effectively with the surface through
355 its available lone-pair electrons, thereby facilitating CO activation.

356 However, our MD results indicate that CO approaches and resides near the surface pre-
357 dominantly in the O-down geometry. This kinetic preference helps explain why CO is dif-
358 ficult to remove during MOR. Although C-down adsorption would be more favorable for
359 oxidation, the pathway by which CO migrates toward the surface naturally drives it into
360 the less-reactive O-down configuration. If the solution-phase migration pathway could be
361 modulated, such as by applying an external electric field to bias the dipole orientation, CO
362 molecules might arrive at the interface with a higher probability of adopting a C-down con-
363 figuration, which could significantly enhance CO oxidation efficiency and thereby improve
364 overall MOR performance.

365 This two-layer adsorption mechanism elucidates how initial C-down attraction facili-
366 tates molecular motion, while surface-parallel orientations at the reaction layer enable effi-
367 cient pathways with minimized CO formation. Moreover, it provides a dynamic perspective
368 that complements classical concepts such as the bifunctional mechanism and d-band the-
369 ory(thermodynamics). From a catalytic design standpoint, these insights highlight the im-
370 portance of engineering electrode surfaces that balance strong initial adsorption with facile
371 reorientation, thereby promoting selective MOR pathways while mitigating CO poisoning.
372 Such a molecular-level understanding bridges dynamic simulation results with a thermody-
373 namic perspective and offers guiding principles for the rational design of advanced FePt-based
374 electrocatalysts.

375 Density functional theory result

376 To complete the entire reaction process and link kinetics and thermodynamics, DFT calcula-
377 tions were performed to complement the MD simulations and provide energetic validation of



378 the observed adsorption configurations. The theoretical calculations were carried out using
379 Density Functional Theory (DFT) with the generalized gradient approximation (GGA) and
380 the Perdew–Burke–Ernzerhof (PBE) exchange–correlation functional in the CASTEP mod-
381 ule of Materials Studio. A 2×2 FePt (111) slab with the $L1_0$ phase structure was constructed
382 to simulate the multistep methanol oxidation reaction (MOR) process on the FePt surface.
383 Different adsorption configurations of CH_3OH and the reaction intermediates were examined
384 to identify the most stable adsorption sites.

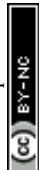
385 A vacuum layer of 20 \AA was introduced to avoid spurious interactions between periodic
386 images along the surface-normal direction. To represent the bulk-like properties of the FePt
387 slab, the bottom two layers were fixed, while the top layer and the adsorbates were fully
388 relaxed. The plane-wave cutoff energy was set to 520 eV, and the Brillouin zone was sampled
389 using a $3 \times 3 \times 1$ Monkhorst–Pack k -point mesh. Structure optimization was performed until
390 the total energy convergence criterion reached 10^{-5} eV. All calculations were spin-polarized.

391 The adsorption free energies of CH_3OH and the reaction intermediates on the FePt slab
392 were calculated according to

$$\Delta E = E_{\text{ads+substrate}} - E_{\text{substrate}} - E_{\text{ads}} \quad (4)$$

393 where $E_{\text{ads+substrate}}$ and $E_{\text{substrate}}$ are the Gibbs free energies of the slab with and without
394 the adsorbate, respectively, and E_{ads} is the Gibbs free energy of the isolated adsorbate.

395 The adsorption energy (E_{ads}) of methanol and its key intermediates was determined on the
396 FePt (111) surface, which provides the most thermodynamically stable adsorption among the
397 examined facets. The details as shown in Fig. 6, CH_2OH , CH_3O , and CO species preferen-
398 tially adopt a C-down orientation at equilibrium, whereas CH_3OH , CH_2O , and CHO species
399 favor O-down adsorption configurations. This trend indicates that both O-down and C-down
400 configurations exist in the methanol oxidation–reduction reaction pathway. Such phenomena
401 indicate that the MOR reaction does not occur solely through C-down or O-down contacts;



402 the configuration of both contacts is crucial. This aligns with our discussion in Section ,
403 where we observed that within the 3 Å range of the inner Helmholtz layer (reaction layer),
404 methanol molecules tend to lie flat to prepare for triggering the next reaction stage. MD
405 simulations reveal a kinetic sequence in which methanol first adsorbs in a C-down orientation
406 and later lies down to the O-down state within the reaction layer. It should be noted that
407 the MD and DFT calculations describe the system under different modeling frameworks and
408 solvation environments. The MD simulations include explicit solvent dynamics and classical
409 force-field interactions, whereas the DFT calculations capture adsorption energetics at the
410 electronic-structure level under more idealized conditions. Therefore, comparisons between
411 MD-derived orientations and DFT-derived adsorption configurations should be interpreted
412 qualitatively and viewed as complementary insights.

413 Linking dynamics with thermodynamics results, we propose a two-layer interfacial mech-
414 anism. In the 5 Å guiding layer, the molecular approach is kinetically steered by carbon-
415 surface attraction, so methanol predominantly displays a C-down orientation while migrating
416 toward the interface. Upon entering the 3 Å reaction layer, molecules adopt a surface-parallel
417 geometry and reorient into O-down configurations, at which point thermodynamics becomes
418 dominant and bond activation is facilitated. Furthermore, the difficulty in removing the
419 poisoning intermediate CO during the MOR process can also be attributed to the kinetically
420 dominated C-down configuration within the 5 Å guiding layer. This orientation favors C-H
421 activation pathways that inevitably promote CO formation at the surface. We propose that
422 modulating the interfacial electric field to induce a transition of surface-parallel methanol
423 molecules in the 3 Å reaction layer toward an O-down orientation could effectively suppress
424 CO accumulation and facilitate its removal, thereby improving catalytic capacity.



425 Conclusions

426 In this work, all-atom classical molecular dynamics simulations were employed to elucidate
427 the dynamic behavior of methanol and co-reactants at FePt electrode surfaces during the
428 MOR. By introducing adsorption time as a quantitative descriptor, we demonstrated that
429 the adsorption times of water, sulfuric acid, and methanol align with their mechanistic roles
430 in the MOR pathway, thereby validating the simulation framework. Furthermore, orientation
431 analysis revealed a two-layer adsorption mechanism in which initial C-down anchoring in the
432 guiding layer drives molecular migration toward the surface, while subsequent reorientation
433 into surface-parallel configurations in the reaction layer enables efficient O-down pathways
434 with minimized CO formation.

435 These findings establish a time-resolved and orientationally resolved picture of molecular
436 adsorption that complements traditional thermodynamic descriptions provided by density
437 functional theory. The results not only provide molecular-level support for bifunctional and
438 *d*-band center concepts in FePt catalysis, but also offer general design principles: effective
439 electrocatalysts should balance strong initial attraction with facile reorientation to promote
440 selective reaction pathways while suppressing poisoning intermediates.

441 Beyond FePt and MOR, the framework presented here highlights the broader potential of
442 adsorption-time and contact-mode analysis to unravel interfacial dynamics in complex elec-
443 trochemical systems. Coupling such molecular dynamics approaches with constant-potential
444 DFT and multiscale models represents a promising direction toward predictive design of
445 next-generation electrocatalysts.

446 Conflicts of interest

447 There are no conflicts to declare.



448 Data availability

449 Data will be made available on request.

450 Acknowledgements

451 This work was supported by the National Natural Science Foundation of China (No. 52271163)
452 and the Fundamental Research Funds for the Central Universities (No. PY2516).

453 Author Contributions

454 Conceptualization: F.Meng, J.L. Liu

455 Methodology: F.Meng, N.Arai

456 Software: F.Meng

457 Validation: F.Meng, J.L. Liu

458 Formal analysis: Meng, Q.Q. Mo, J.L. Liu

459 Investigation: F.Meng, Q.Q. Mo

460 Resources: N.Arai

461 Data Curation: F.Meng, Q.Q. Mo

462 Writing Original Draft: F.Meng

463 Writing Review & Editing: N.Arai, J.L. Liu

464 Visualization: F.Meng

465 Supervision: N.Arai

466 Project administration: N.Arai

467 Funding acquisition: N.Arai, J.L. Liu



468 **References**

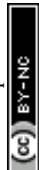
- 469 (1) Phogat, P.; Chand, B.; Shreya.; Jha, R.; Singh, S. Hydrogen and methanol fuel cells:
470 A comprehensive analysis of challenges, advances, and future prospects in clean energy.
471 *International Journal of Hydrogen Energy* **2025**, *109*, 465–485.
- 472 (2) Nørskov, J. K.; Rossmeisl, J.; Logadottir, A.; Lindqvist, L.; Kitchin, J. R.; Bligaard, T.;
473 Jónsson, H. Origin of the Overpotential for Oxygen Reduction at a Fuel-Cell Cathode.
474 *The Journal of Physical Chemistry B* **2004**, *108*, 17886–17892.
- 475 (3) Zhou, K.; Ma, W.; Zeng, Z.; Ma, X.; Xu, X.; Guo, Y.; Li, H.; Li, L. Experimental and
476 DFT study on the adsorption of VOCs on activated carbon/metal oxides composites.
477 *Chemical Engineering Journal* **2019**, *372*, 1122–1133.
- 478 (4) Li, B.; Xiao, C.; Harrison, N. M.; Fogarty, R. M.; Horsfield, A. P. Role of electron
479 localisation in H adsorption and hydride formation in the Mg basal plane under aque-
480 ous corrosion: a first-principles study. *Physical Chemistry Chemical Physics* **2023**, *25*,
481 5989–6001.
- 482 (5) Li, P.; Jiao, Y.; Huang, J.; Chen, S. Electric Double Layer Effects in Electrocatalysis:
483 Insights from Ab Initio Simulation and Hierarchical Continuum Modeling. *JACS Au*
484 **2023**, *3*, 2640–2659.
- 485 (6) Shi, G.; Lu, T.; Zhang, L. Understanding the interfacial water structure in electrocatal-
486 ysis. *National Science Review* **2024**, *11*, nwae241.
- 487 (7) Liu, T.; Chen, Q.-X.; He, Z.; Wang, J.-L.; Sheng, S.-Z.; Liu, J.-W.; Yu, S.-H. Efficient
488 Methanol Oxidation Kinetics Enabled by an Ordered Heterocatalyst with Dual Electric
489 Fields. *Journal of the American Chemical Society* **2025**, *147*, 5340–5349.
- 490 (8) Taheri, Z.; Nakhaei Pour, A. Studying of the adsorption and diffusion behaviors of



- 491 methane on graphene oxide by molecular dynamics simulation. *Journal of Molecular*
492 *Modeling* **2021**, *27*, 59.
- 493 (9) Zhao, H.; Lyu, Y.; Hu, J.; Li, M.; Chen, H.; Jiang, Y.; Tang, M.; Wu, Y.; Sun, W. Re-
494 veal the major factors controlling quinolone adsorption on mesoporous carbon: Batch
495 experiment, DFT calculation, MD simulation, and machine learning modeling. *Chem-*
496 *ical Engineering Journal* **2023**, *463*, 142486.
- 497 (10) Lu, N.; Dong, X.; Chen, Z.; Liu, H.; Zheng, W.; Zhang, B. Effect of solvent on the
498 adsorption behavior of asphaltene on silica surface: A molecular dynamic simulation
499 study. *Journal of Petroleum Science and Engineering* **2022**, *212*, 110212.
- 500 (11) Kinjo, T.; Tsuji, M.; Kusano, T.; Jinnouchi, R.; Makino, S.; Nakamura, H. Effect of
501 substitution degree and dissociation on adsorption behavior of carboxymethyl cellulose
502 on graphite surfaces. *Chemical Physics Letters* **2026**, *883*, 142514.
- 503 (12) Huang, W.; Xu, K.; Liang, L.; Shi, K.; Zheng, Y.; Min, Y.; Cui, Z.; Liu, Q. Tracking
504 methanol oxidation reaction from OH* as guiding agent. *Chemical Engineering Science*
505 **2024**, *292*, 119991.
- 506 (13) Zhang, W.; Huang, B.; Cui, Y.; Shen, L.; Yan, S. Investigation of the mechanism of
507 methanol electrooxidation: a potential-dependent DFT study. *RSC Advances* **2025**,
508 *15*, 11056–11064.
- 509 (14) Li, J.; Yang, F.; Feng, L. Progress of supported Pt-based catalysts for electrochemical
510 methanol energy conversion. *Coordination Chemistry Reviews* **2025**, *534*, 216603.
- 511 (15) Yu, R.; Zhang, Y.; Deng, S.; Zhu, R.; Zhang, S.; Zhang, J.; Zhao, Y.; Xia, Z. Platinum
512 Alloys for Methanol Oxidation Electrocatalysis: Reaction Mechanism and Rational
513 Design of Catalysts with Exceptional Activity and Stability. *Catalysts* **2024**, *14*.



- 514 (16) Berendsen, H.; van der Spoel, D.; van Drunen, R. GROMACS: A message-passing par-
515 allel molecular dynamics implementation. *Computer Physics Communications* **1995**,
516 *91*, 43–56.
- 517 (17) Mo, Q.; Liu, R.; Meng, F.; Juan, Y.; Li, J.; Wang, S.; Arai, N.; Liu, J.; Wang, W.
518 Phase transition and ternary alloying synergistically boosting magnetic field response
519 for methanol oxidation reaction on L10-FeCrPt nanochains. *Applied Catalysis B: En-*
520 *vironment and Energy* **2026**, *387*, 126475.
- 521 (18) Wang, J.; Wolf, R. M.; Caldwell, J. W.; Kollman, P. A.; Case, D. A. Development and
522 testing of a general Amber force field. *Journal of Computational Chemistry* **2004**, *25*,
523 1157 – 1174, Cited by: 15823; All Open Access, Bronze Open Access.
- 524 (19) Kashefolgheta, S.; Wang, S.; Acree, W. E.; Hünenberger, P. H. Evaluation of nine
525 condensed-phase force fields of the GROMOS, CHARMM, OPLS, AMBER, and
526 OpenFF families against experimental cross-solvation free energies. *Phys. Chem. Chem.*
527 *Phys.* **2021**, *23*, 13055–13074.
- 528 (20) He, X.; Man, V. H.; Yang, W.; Lee, T.-S.; Wang, J. A fast and high-quality charge
529 model for the next generation general AMBER force field. *The Journal of Chemical*
530 *Physics* **2020**, *153*, 114502.
- 531 (21) Rappe, A. K.; Casewit, C. J.; Colwell, K. S.; Goddard, W. A. I.; Skiff, W. M. UFF, a full
532 periodic table force field for molecular mechanics and molecular dynamics simulations.
533 *Journal of the American Chemical Society* **1992**, *114*, 10024–10035.
- 534 (22) Gasteiger, J.; Marsili, M. A new model for calculating atomic charges in molecules.
535 *Tetrahedron Letters* **1978**, *19*, 3181–3184.
- 536 (23) Stukowski, A. Visualization and analysis of atomistic simulation data with OVITO-the
537 Open Visualization Tool. *Modelling and Simulation in Materials Science and Engineer-*
538 *ing* **2010**, *18*, 015012.



- 539 (24) Jain, A.; Ong, S. P.; Hautier, G.; Chen, W.; Richards, W. D.; Dacek, S.; Cholia, S.;
540 Gunter, D.; Skinner, D.; Ceder, G.; Persson, K. A. Commentary: The Materials Project:
541 A materials genome approach to accelerating materials innovation. *APL Materials*
542 **2013**, *1*, 011002.
- 543 (25) Horton, M. K. et al. Accelerated data-driven materials science with the Materials
544 Project. *Nature Materials* **2025**, *24*, 1522–1532.
- 545 (26) Zhu, M.; Wang, Y.; Wu, Y.; Liu, J.; Zhang, J.; Huang, H.; Zheng, X.; Shen, J.; Zhao, R.;
546 Zhou, W.; Wang, S. Greatly Enhanced Methanol Oxidation Reaction of CoPt Trun-
547 cated Octahedral Nanoparticles by External Magnetic Fields. *Energy & Environmental*
548 *Materials* **2023**, *6*, e12403, e12403 EEM-2021-0843.R1.
- 549 (27) Dai, W.; Wan, K.; Pang, K.; Guo, J.; Liu, S.; Wu, K.; Tang, C.; Sun, Y.; Shi, X.;
550 Tang, Z.; Long, C.; Dong, F. In-depth understanding and precise modulation of surface
551 reconstruction during heterogeneous electrocatalysis: From model to practical catalyst.
552 *Chem* **2025**, *11*, 102345.
- 553 (28) Liang, J.; Ma, F.; Hwang, S.; Wang, X.; Sokolowski, J.; Li, Q.; Wu, G.; Su, D. Atomic
554 Arrangement Engineering of Metallic Nanocrystals for Energy-Conversion Electrocatal-
555 ysis. *Joule* **2019**, *3*, 956–991.
- 556 (29) Wang, J.; Zhang, B.; Guo, W.; Wang, L.; Chen, J.; Pan, H.; Sun, W. Toward Electrocat-
557 alytic Methanol Oxidation Reaction: Longstanding Debates and Emerging Catalysts.
558 *Advanced Materials* **2023**, *35*, 2211099.
- 559 (30) Dai, S.; Li, M.; Li, H.; Shi, Y.; Zhang, H.; Wang, D.; Xiang, K.; Zou, J.; Luo, G. Ad-
560 vancements in Electrocatalytic Methanol Oxidation: Catalyst Design, Reaction Mech-
561 anisms, and Renewable Energy Applications. *ChemSusChem* **2025**, *18*, e202402767.
- 562 (31) Liu, Y.; Wu, R.; Jin, Y.; Dong, J.; Li, H.; Wang, J. Balancing reactant adsorption for
563 ultra-stable electrocatalytic methanol oxidation reaction. *eScience* **2025**, *5*, 100430.



- 564 (32) He, T.; Wang, W.; Shi, F.; Yang, X.; Li, X.; Wu, J.; Yin, Y.; Jin, M. Mastering the
565 surface strain of platinum catalysts for efficient electrocatalysis. *Nature* **2021**, *598*,
566 76–81.
- 567 (33) Zeng, R.; Yang, Y.; Shen, T.; Wang, H.; Xiong, Y.; Zhu, J.; Wang, D.; Abruña, H. D.
568 Methanol Oxidation Using Ternary Ordered Intermetallic Electrocatalysts: A DEMS
569 Study. *ACS Catalysis* **2020**, *10*, 770–776.
- 570 (34) Seh, Z. W.; Kibsgaard, J.; Dickens, C. F.; Chorkendorff, I.; Nørskov, J. K.;
571 Jaramillo, T. F. Combining theory and experiment in electrocatalysis: Insights into
572 materials design. *Science* **2017**, *355*, eaad4998.
- 573 (35) Hofstead-Duffy, A. M.; Chen, D.-J.; Sun, S.-G.; Tong, Y. J. Origin of the current peak
574 of negative scan in the cyclic voltammetry of methanol electro-oxidation on Pt-based
575 electrocatalysts: a revisit to the current ratio criterion. *Journal of Materials Chemistry*
576 **2012**, *22*, 5205–5208.
- 577 (36) Selivanova, A. V.; Demina, V. G.; Aydakov, E. E.; Saraev, A. A.; Kaichev, V. V.;
578 Bukhtiyarov, V. I. Mechanistic study of methanol oxidation on Pt(111) single crystal.
579 *Applied Surface Science* **2022**, *579*, 152140.
- 580 (37) Chen, W.; Cai, J.; Yang, J.; Sartin, M. M.; Chen, Y.-X. The kinetics of methanol
581 oxidation at a Pt film electrode, a combined mass and infrared spectroscopic study.
582 *Journal of Electroanalytical Chemistry* **2017**, *800*, 89–98, Special Issue in honor of
583 Masatoshi Osawa.
- 584 (38) Li, J.-T.; Chen, Q.-S.; Sun, S.-G. In situ microscope FTIR studies of methanol adsorp-
585 tion and oxidation on an individually addressable array of nanostructured Pt micro-
586 electrodes. *Electrochimica Acta* **2007**, *52*, 5725–5732, Surface Imaging/Spectroscopy at
587 Solid/Liquid Interface (ISSIS).



- 588 (39) Pham, T. L. M.; Vo, D.-V. N.; Nguyen, H. N. T.; Pham-Tran, N.-N. CH versus OH
589 bond scission in methanol decomposition on Pt(111): Role of the dispersion interaction.
590 *Applied Surface Science* **2019**, *481*, 1327–1334.
- 591 (40) Zhang, G.; Schreier, M. Leveraging electrochemical double layer structure to rationally
592 control electrolysis. *National Science Review* **2024**, *11*, nwae299.
- 593 (41) Dourado, A. H. B. Electric Double Layer: The Good, the Bad, and the Beauty. *Elec-*
594 *trochem* **2022**, *3*, 789–808.
- 595 (42) Zhang, X.; Savara, A.; Getman, R. B. A Method for Obtaining Liquid–Solid Adsorption
596 Rates from Molecular Dynamics Simulations: Applied to Methanol on Pt(111) in H₂O.
597 *Journal of Chemical Theory and Computation* **2020**, *16*, 2680–2691.



598 Tables

Table 1: Lattice parameters of the FePt alloy.

Crystal structure	Lattice (Conventional)
Lattice constant a	2.73 Å
Lattice constant b	2.73 Å
Lattice constant c	3.74 Å
Angle α	90.00°
Angle β	90.00°
Angle γ	90.00°
Volume	27.81 Å ³

Table 2: Gaussian fitting parameters (A , μ , and σ) for adsorption time distributions of methanol, sulfuric acid, and water on FePt surfaces.

Surface	Molecule	A	μ (ps)	σ (ps)
(001)	Methanol	0.021	45.583	18.064
	Sulfuric acid	0.044	19.710	9.071
	Water	0.144	11.019	2.619
(100)	Methanol	0.016	53.335	24.135
	Sulfuric acid	0.040	20.381	10.251
	Water	0.117	12.787	3.244
(111)	Methanol	0.018	63.453	20.343
	Sulfuric acid	0.051	20.621	7.286
	Water	0.120	13.893	3.135
(111)-CO	CO	0.028	70.426	13.234
	Sulfuric acid	0.138	13.779	2.627
	Water	0.218	8.865	1.760



599 Figures

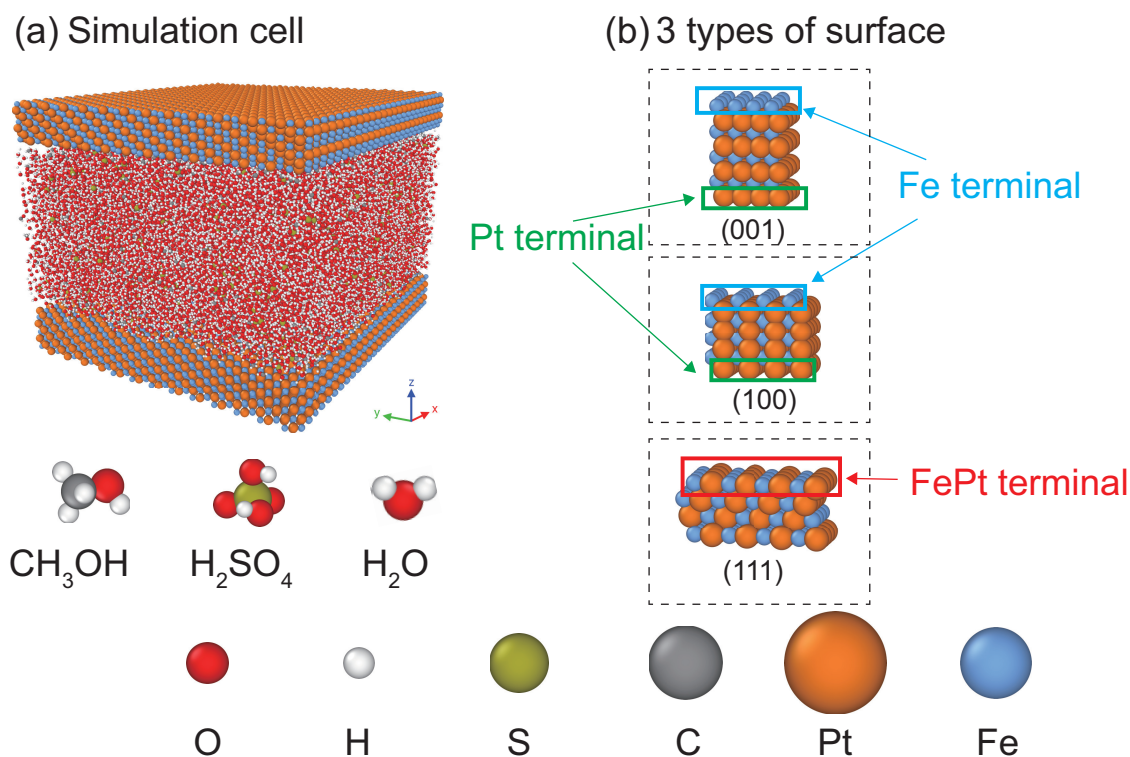


Figure 1: (a) Molecular dynamics simulation box of the FePt electrode-electrolyte interface. The FePt slab is placed at the bottom of the simulation box and exposed to a mixed electrolyte containing methanol (CH₃OH), sulfuric acid (H₂SO₄), and water (H₂O). Periodic boundary conditions are applied in all directions. (b) Surface atomic structures of FePt with different Miller indices. For the (001) and (100) facets, two distinct terminations are present, corresponding to Pt-terminated and Fe-terminated surfaces. In contrast, the (111) facet exposes a mixed Fe-Pt termination. Atom colors: O (red), H (white), S (yellow), C (gray), Pt (orange), and Fe (blue).



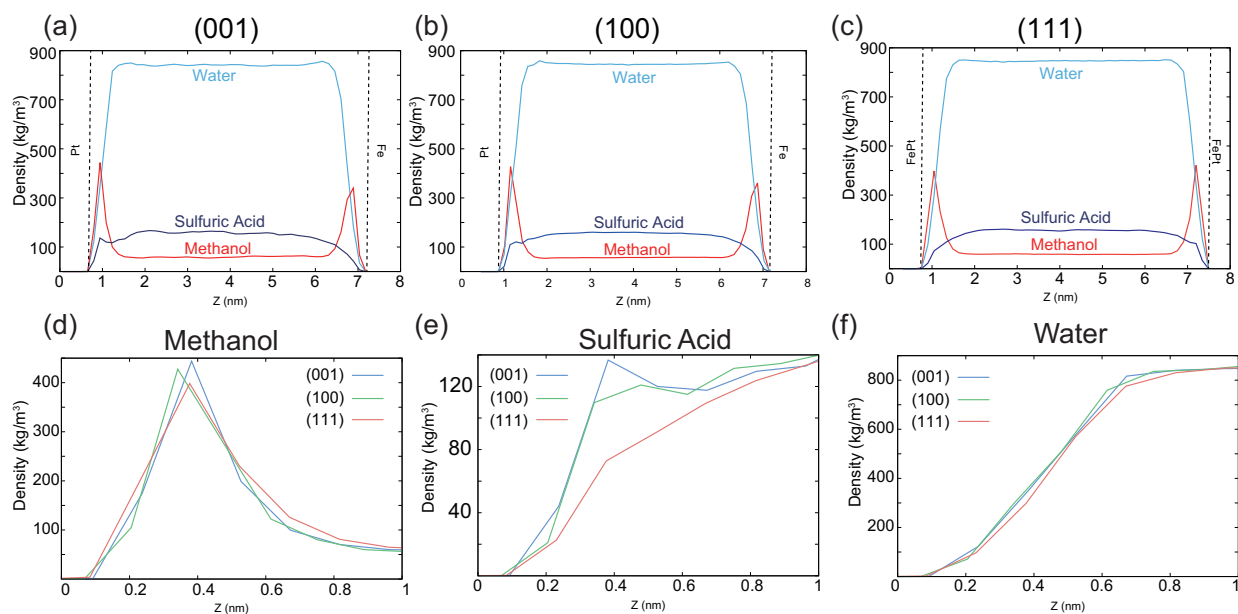


Figure 2: Density distributions of methanol, sulfuric acid, and water along the Axis-Z for FePt surfaces with different Miller indices. (a-c) Density profiles across the entire simulation box for the (001), (100), and (111) surfaces, respectively. (d-f) Enlarged density profiles within 1.0 nm from the Pt-contact surface, highlighting the near-surface distributions of methanol, sulfuric acid, and water for different surface orientations.



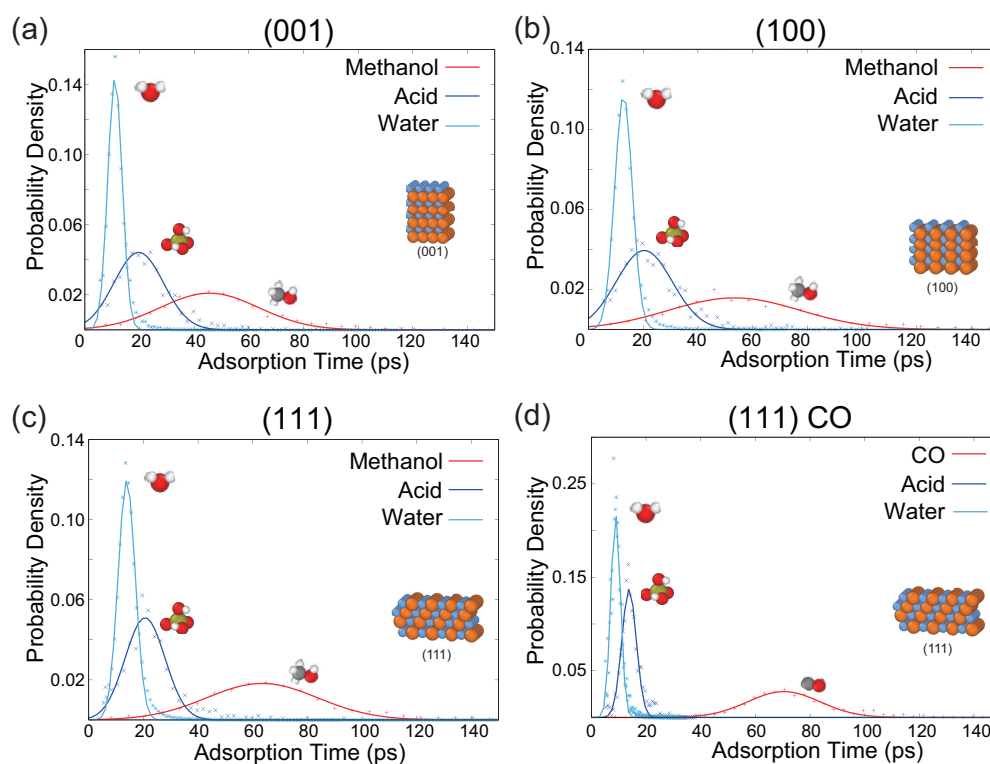


Figure 3: Probability density distributions of adsorption times for different species on FePt surfaces with different Miller indices. (a-c) Adsorption time distributions of methanol, sulfuric acid, and water on the (001), (100), and (111) surfaces, respectively. Adsorption time is defined as the continuous residence duration of a molecule within 1 nm of the catalyst surface. Solid lines represent Gaussian fits to the probability density distributions. (d) Adsorption time distributions of CO, sulfuric acid, and water on the FePt (111) surface, illustrating the competitive adsorption behavior induced by strong CO binding. The results reveal distinct residence-time hierarchies among different species and highlight the prolonged surface occupation of CO on the (111) facet.



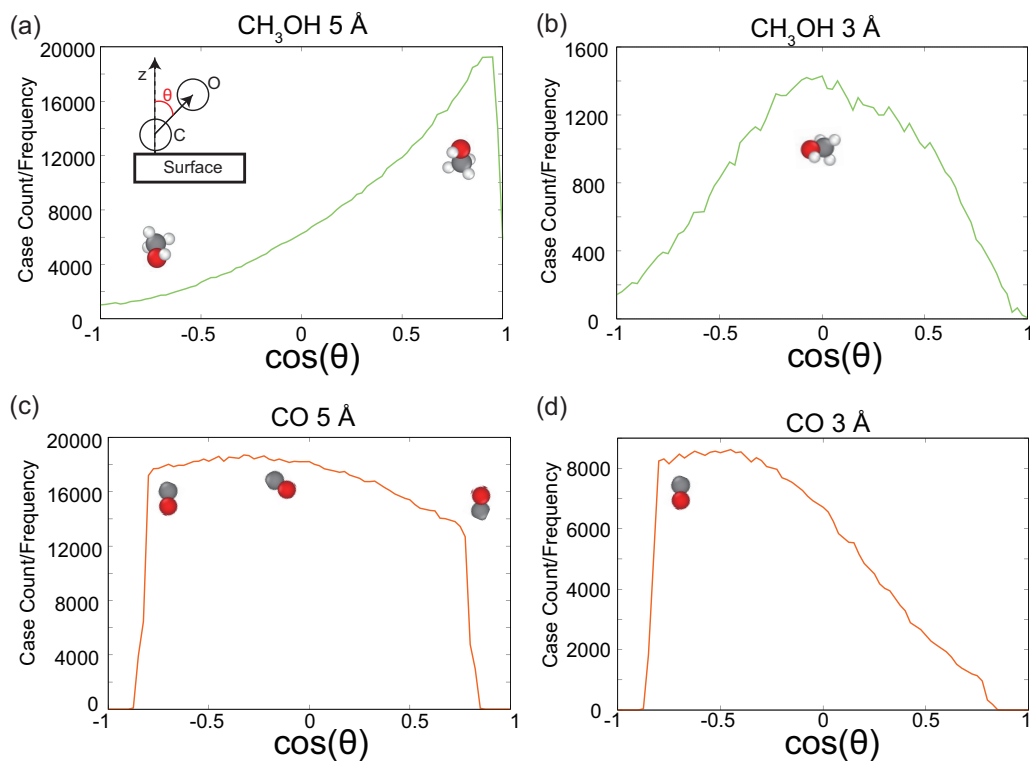


Figure 4: Orientation distributions of methanol and CO near the FePt (111) surface, expressed as $\cos\theta$, where $\cos\theta$ is the angle between the molecular bond vector and the surface normal. (a,b) $\cos\theta$ distributions of methanol at distances of 5 Å (guiding layer) and 3 Å (reaction layer) from the surface, respectively. At 5 Å, methanol exhibits a pronounced preference for C-down orientations, whereas at 3 Å the distribution becomes nearly symmetric around $\cos\theta = 0$, indicating a surface-parallel configuration. (c,d) $\cos\theta$ distributions of CO at 5 Å and 3 Å from the surface, respectively. In contrast to methanol, CO predominantly adopts O-down orientations in both layers, suggesting kinetically favored configurations that are less conducive to CO bond activation and oxidation.

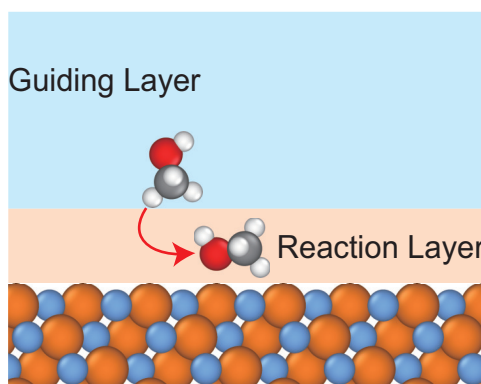


Figure 5: Schematic illustration of the two-layer interfacial adsorption model.



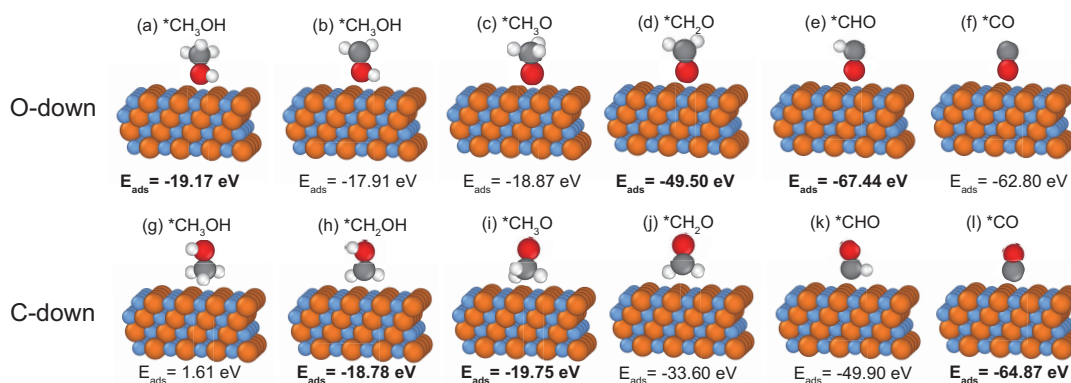


Figure 6: DFT-optimized adsorption configurations and adsorption energies (E_{ads}) of methanol and key MOR intermediates on the FePt(111) surface. Panels (a-f) show O-down adsorption geometries, while panels (g-l) present the corresponding C-down configurations. The results indicate that both C-down and O-down adsorption modes coexist along the reaction pathway, reflecting the accessibility of multiple adsorption orientations during MOR.



Data Availability Statement

The datasets supporting the findings of this study, including molecular dynamics and density functional theory results, are available from the corresponding author upon reasonable request.

